Performance of High-Modulus Near-Surface-Mounted FRP Laminates for Strengthening of Concrete Columns

Article *in* Composites Part B Engineering · November 2018

DOI: 10.1016/j.compositesb.2018.11.064

2 authors:

Koosha Khorramian
Dalhousie University
11 PUBLICATIONS **27** CITATIONS
SEE PROFILE

Pedram Sadeghian
Dalhousie University
60 PUBLICATIONS **207** CITATIONS
SEE PROFILE

Performance of High-Modulus Near-Surface-Mounted FRP Laminates for Strengthening of Concrete Columns

Koosha Khorramian[1] and Pedram Sadeghian[2]

ABSTRACT: This study investigates the performance of high-modulus near-surface-mounted (NSM) fiber-reinforced polymer (FRP) laminates in strengthening of existing concrete columns. The focus of this study is on the compressive and buckling characteristics of carbon FRP (CFRP) laminates installed on short columns for strengthening to validate their sufficiency for further studies on slender columns. In this paper, an experimental study was designed to consider the effect of eccentric loading on short concrete columns (500×150×150 mm^3) strengthened with four longitudinal NSM CFRP laminates (1.2×10 mm^2). All specimens were tested symmetrically under the eccentricity to width ratios of 0, 10, 20, and 30% to give a single curvature bending combined with axial load. The experimental results showed no buckling/debonding failure of CFRP laminates, while some of the CFRP laminates reached to crushing points long after the peak load. Moreover, material coupon tests showed that the strength and elastic modulus of the CFRPs in compression were 34% and 86% of those in tension, respectively. The average compressive strain of NSM CFRP laminates for all column specimens under eccentric loading at peak load and after 15% drop from the peak load was 41% and 84% of their ultimate compressive strain obtained from compression coupon tests, respectively. Furthermore, a robust analytical model was developed considering the material and geometrical nonlinearities and it was verified against experimental results. Overall, the results indicated that strengthening short concrete columns with NSM CFRP

[1] PhD Student, Department of Civil and Resource Engineering, Dalhousie University, 1360 Barrington street, Halifax, NS, B3H 4R2 Canada.
[2] Assistant Professor and Canada Research Chair in Sustainable Infrastructure, Department of Civil and Resource Engineering, Dalhousie University, 1360 Barrington Street, Halifax, NS, B3H 4R2 Canada. Email: Pedram.Sadeghian@dal.ca (corresponding author)

laminates improved the capacity of the columns without any premature buckling, debonding, or crushing of CFRP laminates. The results will open new avenues in the FRP strengthening of concrete columns, especially slender columns, where the high-modulus NSM system can also enhance the lateral stiffness of the columns for buckling control.

https://doi.org/10.1016/j.compositesb.2018.11.064

KEYWORDS: CFRP, NSM, Laminate, Column, Concrete, Experimental, Analytical.

1. INTRODUCTION

In the past decades, researchers have studied the effectiveness of near-surface-mounted (NSM) fiber-reinforced polymer (FRP) laminates for strengthening of existing reinforced concrete (RC) beams. The NSM technique, like externally bonded FRP (EBF) technique, has been implemented to the tension side of concrete beams. In contrast to EBF sheets, NSM FRPs are inserted into grooves created in the concrete cover of concrete beam using an adhesive. Moreover, NSM technique provides more surfaces of concrete in interaction with adhesives which makes debonding less conceivable in comparison to the EBF technique. There have been considerable researches on the behavior of NSM FRP reinforcements for strengthening concrete beams [1, 2, 3, 4] and concrete slabs [5, 6], however, a few researches have been conducted on NSM FRP applications on columns [7, 8, 9].

NSM FRP laminates has not been used for strengthening concrete columns because it is believed that they are not efficient in compression. For example, Fib Bulletin 14 [10] mentioned that the modulus of elasticity of FRP in compression is lower than its modulus in tension. ACI 440.2R [11] emphasized that the usage of FRP systems as compressive reinforcement is not recommended. CAN/CSA S806 [12] clarified that FRP reinforcing elements in concrete

compression zone shall be deemed to have zero compression strength and stiffness for design purposes. The use of FRPs in compression is not recommended by ACI 440.2R [11] because of possible premature failures such as micro buckling of fibers, buckling of unsupported or poorly supported laminates, and improperly anchorage of substrate and FRP surface as well as unreliability in the compressive strength of laminates. Micro buckling could arise from performing weak quality control of the FRP production which is attributed to the presence of voids in the resin by ACI 440.2R [11], although commitment in quality control can fix this problem.

On the other hand, Barros et al. [9] performed a numerical and experimental investigation to evaluate the effectiveness of NSM carbon FRP (CFRP) strips on the flexural strengthening of RC columns whose result showed a significant increase of load carrying capacity of columns failing in bending. In another study, Gajdosova and Bilcik [8] studied slender RC columns strengthened with NSM CFRPs experimentally and found that resistance enhancement is achieved for both short and slender concrete columns. Sadeghian and Fam [13] investigated the application of high-modulus externally bonded longitudinal FRPs on slender RC columns which showed that by applying longitudinal FRP laminates, the loading path of slender columns is improved to gain higher axial capacity due to the additional gain in stiffness of columns. Regarding the neglection of FRP laminates in compression on one hand and their effectiveness in compressive behavior on the other hand, the compressive behavior of NSM FRPs in compression needs to be investigated in depth. There are insufficient researches on the adequacy of longitudinal compressive NSM FRP laminates in both flexural and axially loaded concrete columns in terms of their strength and stiffness which requires a better knowledge of behavior of FRPs in compression. Moreover, the possibility of premature crushing, debonding, buckling failures of NSM FRP-strengthened concrete columns indicates the necessity of more studies in this field. Addressing these issues

requires compression tests with high degree of accuracy. Therefore, the current research tries to address some of these vague prospective problems.

This research was designed to evaluate the behavior of NSM CFRP strips used for strengthening of short concrete columns under eccentric and concentric loadings using experimental and analytical methods. The experimental program consists of fourteen medium-scale concrete columns strengthened with NSM CFRP strips and tested under single curvature bending and compressive axial loads. The analytical part includes a verified model which considers the nonlinearity of both geometry and material and predicts the behavior of these columns. Furthermore, a parametric study performed to provided supporting information about the compressive behavior of NSM CFRP strengthened short concrete columns. This study is a part of a comprehensive project on application of longitudinal FRPs in concrete columns, especially slender columns. The authors believe that high-modulus NSM FRPs can be effective for strengthening of slender RC columns through enhancing the lateral stiffness of the columns. The results of this study will establish a data platform on compressive behavior of NSM FRPs for more in-depth studies on strengthening of slender RC columns.

2. EXPERIMENTAL PROGRAM

In this section, the experimental program consisting of fourteen medium-scale short concrete columns tested under concentric and eccentric loads is explained, where nine of these specimens were reinforced with NSM CFRP laminates. In the following, the test matrix, material properties, fabrication, and test set up for both plain and reinforced concrete column specimens are explained.

2.1. Test Matrix

A total of fourteen 500 mm long concrete columns with a square cross-section (150×150 mm^2) were prepared and tested under pure axial and combined flexural and axial loadings. Nine of these specimens were strengthened with NSM CFRP laminates. Four specimens consisting two plain concrete and two specimens strengthened with NSM CFRP laminates were tested under concentric axial load and other specimens were tested under eccentric loads at 15, 30, and 45 mm, i.e. 10, 20, and 30 percent of width of the cross-section, respectively, as presented in Table 1. It should be noted that for the sake of simplicity and focusing on the modes of failure of NSM reinforcement, the plain concrete specimens were considered to be reinforced only with NSM FRPs. Moreover, studying only plain concrete and FRPs highlights the effect of NSM FRPs even for strengthening cases in which the longitudinal steel reinforcement would not be effective structurally anymore due to corrosion. To name the specimens, a label like "A-ex-y" was used where A, x, and y indicate the column type, the eccentricity, and the specimen number, respectively. The column type is identified by "P" for plain or "N" for NSM CFRP strengthened concrete columns.

2.2. Material Properties

The concrete was ready-mixed and the maximum aggregate size was 12.5 mm. The compressive strength of concrete at the time of testing of columns measured as 37.0±0.8 MPa using three concrete cylinders (100 mm diameter and 200 mm height). To strengthen concrete specimens, pre-manufactured unidirectional CFRP strips with a thickness and width of 1.2 and 10 mm, respectively, were used. The NSM CFRP strips were inserted in grooves using a compatible adhesive for bonding purpose. The tensile strength, compressive modulus of elasticity, tensile rupture strain, and bond strength of adhesive were reported by manufacturer as 27.06 MPa, 3.06 GPa, 0.01 mm/mm, and 13.8 MPa, respectively.

The tensile characteristics of CFRP strips were also evaluated by testing five tensile coupons prepared per ASTM D3039/D3039M [14]. The average ± standard deviation of ultimate tensile strength, tensile modulus of elasticity, and rupture strain of tested specimens were 3006±288 MPa, 180.5±8.3 GPa, and 0.01668±0.00176 mm/mm, respectively. The stress-strain behavior of CFRP laminates in tension was linear as shown in Figure 1(a).

To assess the compressive characteristics of the CFRP laminates, five compressive coupons were prepared and tested under pure compressive load using a test fixture that was prepared per ASTM D6641/D6641M [15]. Width and thickness of each compressive coupon was 1.2 and 12.2 mm, respectively, while the length of each coupon was 216 mm which was tabbed with two 102 mm long CFRP strips at each end so that the free length of the specimen was 12 mm as shown in Figure 2(a). The test fixture consists of two thick steel cubes which can move using two alignment rods, two thick steel plates that holds the specimen in place during testing, and four patterned steel tabs to decrease the chance of premature failure, as shown in Figure 2(b). It should be noted that the tests were performed using displacement control approach with a rate of 0.5 mm/min. All the specimens were crushed in the gauge length as presented in Figure 2(c). No buckling was observed during the test, and all specimens failed with a crushing failure mode in the gauge length. This failure is described by ASTM D6641/D6641M [15] as the transverse shear or through thickness failure modes at grip/tab on top (TAT or HAT) as shown in Figure 2(d).

The average ± standard deviation of ultimate compressive strength, compressive modulus of elasticity, and crushing strain of tested specimens were 1031±47 MPa, 156.1±5 GPa, and 0.0066 mm/mm, respectively. The crushing strain was derived by division of average compressive strength to modulus of elasticity of the compressive coupons. For capturing strains, two strain gauges were installed on the gauge length of the coupons, and the average strain for each coupon

represented the stress-strain curves. The stress-strain behavior of CFRP laminates in compression was linear as shown in Figure 1(b).

The average strength of the tested CFRP coupons in compression was 34% of the average strength of the coupons in tension. The average compressive strength was considerably lower than the tensile strength of CFRP laminate, however, it should be considered that the strength is still considerably high (1031 MPa) which is more than two times higher than conventional steel rebar. It was observed that the average modulus of elasticity of the CFRP coupons in compression was only 86% of the average modulus of elasticity of the coupons in tension. Although the average crushing strain of the CFRP coupons was 0.0066 mm/mm (60% of the average rupture strain in tension), it is still almost two times higher than the design crushing strains of concrete, i.e. 0.003 and 0.0035 mm/mm defined by ACI 318 [16] and CSA A23.3 [17], respectively. Therefore, material tests showed proper characteristics for CFRP laminates in compression for structural usage purposes.

2.3. Fabrication

To provide the concrete specimens with proper grooves for NSM strips, four wooden strips with width and thickness of 15 mm and 5 mm, respectively, were attached to each wooden mold. The method of creating the grooves in fresh concrete was selected for the laboratory safety reason instead of cutting the grooves in hard concrete using concrete saw. The wooden strips were hold in place using both adhesive in the longitudinal direction and four holes at the ends of molds as shown in Figure 3(a). The clear distance between wooden strips was 30 mm and their distance from the edges of molds was 55 mm. All concrete specimens were casted with a ready-mix concrete as shown in Figure 3(b). The specimens cured at the room temperature and saved their moisture using plastic covers shown in Figure 3(c). In fourteen days after pouring concrete, the

wooden molds were removed from the specimens [Figure 3(d)], and grooves were prepared for mounting of CFRP strips by cleaning and grinding the interior surface of grooves which gave a better friction between bonding agent and concrete surface as well as removing dust and wood particles from grooves, as presented in Figure 3(e).

For each side of every specimen, a strain gauge installed on the surface of NSM CFRP strip [Figure 3(f)] which was coated with nitrile rubber coating agent and covered by aluminum tape. The CFRP strips were embedded in the grooves of concrete specimens using a compatible adhesive as bonding material as is shown in Figure 3(g). To avoid prospective premature failure caused by load concentration at the ends of specimens which are close to the load application point, both ends of the specimens were wrapped with two layers of unidirectional basalt fabrics and epoxy resin as shown in Figure 3(h). The top and bottom of each specimen then grinded to give a flat column end surface.

2.4. Test Set Up

The test set up and instrumentation of specimens used in this study are presented in Figure 4(a). Two steel caps were installed on top and bottom of each specimen provided both load eccentricity and simply supported condition for the specimens tested under combined flexural and axial loads. As shown in Figure 4(b), each steel cap was created by welding a 30-mm thick steel plate, with a V-shape notch, on top of a square steel plate with width and thickness of 250 mm and 10 mm, respectively. For testing specimens under different load eccentricities, the location of notched plate altered to meet new eccentricity demand by removing welds and rewelding them in the new location. Two steel cylinders attached to the testing machine upon which the notched steel caps stands and provide the rotation at the ends of specimens so that pin-pin testing condition satisfied, as shown in Figure 4(b). The symmetricity of steel cylinders and notches at the ends of the

specimens made columns experience single curvature bending. To ensure that steel caps and specimens rotating together without sliding on each other, four steel angle profiles surrounded the specimen circumference at both ends and attached to the steel cap using bolt fasteners, as presented in Figure 4(b). To increase the degree of integration between steel cap and specimens, before fastening the adjustable steel angles to the steel cap, a plastic bag filled with quick set fresh grout placed on top of specimen so that it covers the interface of concrete column, steel cap, and angles.

The final position of the specimen with steel cap after putting inside the 2 MN universal testing machine is shown in Figure 3(a). The instrumentation designed to capture longitudinal strain of CFRP strips at both compressive and tensile sides using strain gauges one strain gauge at each side on the surface of CFRP strip (i.e. SG 1 and SG 2) as well as recording the lateral displacement of specimens at the mid height of columns using two horizontal linear variable differential transformers (LVDTs) on compressive (i.e. LVDT 3) and tensile side (i.e. LVDT 4), as shown in Figure 4(b). To secure the data recorded by strain gauges, two vertical LVDTs (i.e. LVDT 1 and LVDT 2) were installed at the mid height of specimens on the concrete surface by an aluminum plate holding each strain gauge and adhered to concrete surface. On top of these LVDTs, two aluminum angles were glued to the concrete surface to provide a gauge length of 100 mm as shown in Figure 4(a) and 4(b). All tests were conducted using displacement control approach with a loading rate of 0.625 mm/min and data acquisition rate of 10 data point per second.

3. EXPERIMENTAL RESULTS AND DISCUSSION

The experimental result of the tests conducted in this study, consisting of fourteen short specimen columns are discussed in this section starting from failure modes description, passing to the

behavior of NSM CFRP laminates in compression, and concluding with their effect on the load bearing capacity of the tested columns. A summary of test results is shown in Table 2.

3.1. Failure Mode

Overall, four modes of failure were observed in reinforced specimens consisting of concrete spalling (CS), concrete crushing (CC), compressive FRP crushing (CFC), tensile FRP rupture (TFR), however, no buckling or debonding of NSM FRP strips observed during the tests. Concrete spalling (CS) happened about the peak load or at peak load where the compressive stresses in concrete were critical and cracks caused the separation of a concrete segment in compressive side of the specimens, as is shown in Figure 5(a). It was observed that the average compressive strain of CFRP at peak load for 0, 10, 20, and 30 percent eccentricity to width ratios, were 0.00156, 0.00270, 0.00329, and 0.00327 mm/mm, respectively, which result in 0.0027 mm/mm as the average of compressive strain of CFRP in compression. Therefore, at peak load, the compressive strain of concrete was close to 0.003 mm/mm or 0.0035 mm/mm that justifies the observation of concrete spalling about the peak load. Concrete crushing (CC) defined where the strain of furthest compressive fiber in concrete reached 0.003 mm/mm or 0.0035 mm/mm, which were the ultimate design strain of concrete introduced by ACI 318 [16] or CSA A23.3 [17], respectively. The compressive FRP crushing (CFC), which is presented in Figure 5(b), happened long after the peak load with a noise and sudden appearance of crack on the surface of adhesive. The tensile cracks shown in Figure 5(c) happened prior to tensile FRP rupture (TFR) which was sudden and with noise, as shown in Figure 5(d).

For both plain concrete and strengthened specimens tested under pure compression, the mode of failure was concrete spalling (CS). For NSM specimens tested with 10 percent eccentricity to width ratio [Figure 6(a)], first concrete spalling (CS) happened followed by crushing of at both

CFRP strips in compressive zone (CFC). Because the concrete spalling and crushing of CFRP strips for all strengthened specimens happened nearly at the mid-height of column except N-e10-2, it was recognized as premature failed specimen and its results were removed from the rest of this study. As shown in Figure 6(b), both strengthened specimens tested under 20 percent eccentricity to width ratio, crushing of one of CFRP strips under compression (CFC) observed followed by concrete spalling (CS). As shown in Figure 6(c), N-e30-1 specimen experienced spalling (CS) and crushing of concrete (CC) before crushing of one of the compressive strips (CFC) while for N-e30-2, the tensile CFRP rupture (TFR) happened followed by concrete spalling (CS) and crushing of one compressive CFRP strip (CFC). It should be noted that this failure modes were observed after the peak load, however, up to the peak load, no rupture, crushing, debonding, or buckling of CFRP strips were observed.

3.2. Compressive Behavior of NSM CFRPs

Overall, all NSM CFRP strips of the specimens tested under eccentric loading, experienced considerable compressive strains without debonding and/or buckling. The strain of CFRP strips recorded by strain gauges for eccentrically loaded specimens is drawn in Figure 7(a). It was observed that as the load eccentricity increases, the peak load decreases. Moreover, Figure 7(a) shows that compressive CFRP strips experienced higher levels of strain in comparison to tensile strips. The average of strain of CFRP strips at tension side (SG1) as well as compression side (SG2) at peak load and a defined ultimate level are presented in Table 2. To define a criterion for the ultimate strain of CFRP strips, the strain values at loads corresponding to 15 percent drop after peak load were considered as the ultimate values which is similar to the one used in a study performed by Hognestad for concrete [18]. Table 2 shows that the tensile strain of the CFRP strips did not reach 14% of the rupture strain, while for compression strips the compartment strain was

50% of the crushing strain obtained from material test. This infers that the behavior of the CFRP strips are more critical when used in compression than when used in tension, however, up to peak load the CFRP strips worked effectively. Moreover, in average the CFRP strips in tension reached 4%, 7%, and 29% of their rupture strain for specimens tested under 0.1, 0.2, and 0.3 eccentricity-to-width ratios, respectively, while the strips in compression reached 86%, 77%, and 90% of their crushing strain, respectively, for the mentioned eccentricities. Overall, the average compressive strain of CFRP strips for all tested specimens was 41% and 84% of their crushing strain at peak load and after 15% drop from the peak load, respectively. Moreover, for CFRP strips in compression, the results showed no evidence of buckling or debonding of CFRP strips before compressive crushing. The latter shows the NSM technique limit the behavior of CFRP strips so that the ultimate material capacity, or crushing, controls the failure mode. Therefore, CFRP strips in compression were able to sustain strains up to their crushing capacity using the NSM technique without any buckling for both eccentric and concentric loadings which shows their effectiveness and capability in strengthening of compressive members.

3.3. Effect of NSM CFRPs on Load Bearing Capacity of Columns

As it is shown in Table 2, the load carrying capacity of plain concrete specimens enhanced by installing NSM CFRP strips in both pure compression and combined axial and compressive loading cases. The load capacity of NSM-strengthened specimens tested under concentric and 10 percent eccentricity were 7.7 and 10.9% higher than their corresponding plain specimens. Also, for NSM-strengthened specimens, as the load eccentricity increases to 10, 20, and 30%; the load capacity decreases 14.6, 29.6, and 48.5% with respect to the specimens under concentric loading, respectively. Figure 7(b) presents the load-displacement diagrams of eccentrically loaded specimens using the average values of LVDT 3 and LVDT 4 as the lateral displacement at the mid-

height of the columns. It is seen that in higher eccentricities, the stiffness of strengthened specimens, which is defined as the slope of load-deflection curves, decreases as well as the axial capacity of columns.

4. ANALYTICAL STUDIES

In order to analyze the results of experimental program, an analytical model was developed which considers the nonlinear behavior of material as well as geometry, using MATLAB software. The model predicts the compressive and tensile strains of the NSM FRP strips, deflection at the mid-height of columns, and second-order moments. This section begins with a description of the model and major assumptions in developing it, followed by verification of the model and eventually concluded by a parametric study.

4.1. Model Description

The program progress by changing the values of compressive load in some steps up to failure and find the corresponding lateral displacement and strains by satisfying equilibrium equation for both internal and external forces. The model considers pin-pin boundary condition as well as the same load (P) and initial eccentricity (e_0) at both ends of column which gives the symmetry of load and boundary condition. The model divides the column length into three nodes, one at the mid-height of column and two at the ends of column. Figure 8 provides the schematic illustration of the process through which the displacement at mid-height of column is determined. At each load step, an arbitrary displacement assumed as the displacement of the middle node of column, as shown by Δ in Figure 8(a). Having known displacement, the total eccentricity of middle node is the summation of the displacement and the initial eccentricity ($e = e_0 + \Delta$), and the corresponding bending moment is the product of the total eccentricity and the given load ($M = Pe_0 + P\delta$) as illustrated

in Figure 8(b). The curvature of end nodes (ψ_0) and middle node (ψ_m), whose diagram is depicted in Figure 8(c), is calculated using the moment-curvature diagram of the cross section at each certain load from the moment at end nodes (M_0) and at middle node of column (M), respectively. In this model, the shape of curvature diagram is assumed as a sine function [Equation 1-a] from which by applying the moment-area theorem [Equation 1-b], the deflection at the mid-height of the column is determined.

$$\psi(y) = (\psi_m - \psi_0) sin\frac{\pi y}{L} + \psi_0 \tag{1-a}$$

$$\delta_m = \int_0^{L/2} y\psi(y)dx = (\psi_m - \psi_0)\int_0^{L/2} ysin\frac{\pi y}{L}dx + \int_0^{L/2} y\psi_0\, dy \tag{1-b}$$

The symbols used in Equation 1 are y, ψ_0, ψ_m, $\psi(x)$, and δ_m which present the distance from the top of column, the curvature at the end of column, the curvature at the middle of column, curvature at x from the top of column, and the displacement of column at its mid-height, respectively, as shown in Figure 8. The assumed shape of curvature function and, in turn, displacement diagram, was adopted from Broms and Viest [19], Lloyd and Regan [20], Claeson and Gyltoft [21] for steel reinforced concrete columns, as well as from Sadeghian et al. [13], and Mirmiran et al. [22] for externally FRP-bonded RC columns and GFRP-reinforced concrete columns, respectively. However, the mentioned models focused on the column capacity while the developed model in this study predicts the strains of compressive and tensile FRP reinforcements, lateral deflection at mid-height of column as well as the loading path and moment-curvature of the NSM FRP columns.

At the stage that the deflection of the middle node is calculated, the calculated value is compared to the initial assumed deflection. An iterative process through which displacement alters until the initial value and the calculated value based are the same implements to find the

corresponding displacement of the column including second order effects. The explained process requires the knowledge moment-curvature diagram of the cross-section which is just a characteristic of loading and cross-section but not the length and displacement of the column.

The moment-curvature diagram for a given load (P) and cross-section is essentially calculated based on the equilibrium of internal forces. In this study, a square concrete cross-section and four NSM CFRP reinforcement were used as shown in Figure 9(a). The width and height of cross-section are called *b* and *h*, respectively, while the distance between the furthest compression fiber (the top edge of concrete) to the top and bottom center of NSM CFRP layers are *d* and *d'*, respectively, as shown in Figure 9(a). The strain profile assumed to be linear in the section which is compatible with the major assumption that transverse plane sections remain plane after bending. The strain of concrete at the furthest compressive fiber, the strain of compressive NSM CFRP (at top), and the strain of tensile NSM CFRP layer (at bottom), at their centers, are presented by ε_{cmax}, ε_{cf}, and ε_{tf}, respectively [Figure 9(b)]. The depth of neutral axis (N.A.) and the curvature are presented as *C* and ψ, respectively [Figure 8(a)], which related to each other by Equation 2.

$$\psi = \frac{\varepsilon_{cmax}}{C} \tag{2}$$

To derive the curvature for a given load (P) and eccentricity (e), which is measured from the center of the section [Figure 9(c)], an iterative process is involved, where ε_{cmax} is assumed and the depth of neutral axis (C) is determined by satisfying force and moment equilibrium for internal forces as well as the external load (P) presented in Equation 3. If the equilibrium equations are not satisfied by changing the depth of neutral axis, the iterative process continues by assigning new values to ε_{cmax} and a new try for finding the depth of neutral axis until equilibrium equations [Equation 3] is satisfied, which is presented in the following:

$$\sum F = 0 \quad \rightarrow \quad P = C_f + C_c - T \tag{3-a}$$

$$\sum M_A = 0 \quad \rightarrow \quad P \times \left(d - \frac{h}{2} + e\right) = C_f \times (d - d') + C_c \times (d - a) \tag{3-b}$$

where C_c, C_f, T, and a are the resultant of compressive stresses of concrete, the internal compressive force in NSM CFRP (top layer), the tension force in NSM CFRP (bottom layer), and the center of application of internal compressive stresses of concrete. It is noticed that the value of T, considered positive (in Equation 3) if the bottom NSM CFRP layer is in tension and negative if the mentioned layer is in compression. The tensile stresses are concrete are very small values, therefore, their contribution in the equilibrium equations are negligible in comparison to the tension stresses sustained by NSM CFRP, and as a result the stress of concrete fibers in tension considered as zero.

The forces of NSM CFRP layers (i.e. C_f and T) are calculated as the production of total area and the stress of the CFRP layer [Equation 4]. For concrete, the compression zone, from neutral axis to the edge of cross section, is divided into rectangular layers with a height of 0.25 mm and the same width as the section. The compressive Force of concrete (i.e. C_c), then, is calculated as the sum of forces from each layer as presented in Equation 5-a, and the center of application of concrete compressive force (i.e. a), determined by Equation 5-b, in which the stress of compressive NSM CFRP layers are subtracted in both formulas.

$$C_s = f_{f1} A_{f1} \quad , \quad T = f_{f2} A_{f2} \tag{4}$$

$$C_c = \sum \frac{1}{2}\left(f_{c_i} + f_{c_{i+1}}\right) b \delta_y - \sum \frac{1}{2}\left(f_{c_i} + f_{c_{i+1}}\right) A_{fi} \tag{5-a}$$

$$a = \frac{1}{C_c}\left[\sum \frac{1}{2}\left(f_{c_i} + f_{c_{i+1}}\right) b \delta_y \bar{y}_{c_i} - \sum \frac{1}{2}\left(f_{c_i} + f_{c_{i+1}}\right) A_{fi} y_{f_i}\right] \tag{5-b}$$

In Equations 4 and 5, the stress and the corresponding sectional areas of each NSM CFRP layer is presented as f_{fi} and A_{fi}, where index i can take value of 1 or 2 for top or bottom layers. Moreover, the stress at bottom and top, width, height of each concrete layer, and the distance between the center of each concrete layer to the neutral axis are named f_{c_i} and $f_{c_{i+1}}$, b, δ_y, and $\bar{y}_{c_i}$, respectively. The stresses introduced in Equation 4 and 5 are calculated from the stress strain relationship for CFRP and concrete material.

The stress-strain relationship of CFRP and concrete material used in this analysis is shown in Figure 10. The CFRP material considered to have the different modulus of elasticity and strength in tension (E_{ft}, f_{ftu}) and compression (E_{fc}, f_{fcu}). The CFRP stress-strain material property was considered linear from zero up to rupture strain (ε_{ftu}) in tension or crushing (ε_{fcu}) in compression. For concrete, the tensile stresses considered as zero for the sake of simplicity while the Popovics [23] stress-strain relationship was considered for the compressive part. The following equations shows Popovics curve:

$$f_c = \frac{f_c' \left(\varepsilon_c / \varepsilon_c'\right) r}{r - 1 + \left(\varepsilon_c / \varepsilon_c'\right)^r} \tag{6-a}$$

$$r = \frac{E_c}{(E_c - E_{sec})} \tag{6-b}$$

$$E_{sec} = f_c' / \varepsilon_c' \tag{6-c}$$

where f_c' is concrete strength and ε_c' is its corresponding strain. Moreover, f_c, ε_c, and E_c are defined as the concrete stress, strain, and modulus of elasticity, respectively. To calculate the modulus of elasticity of concrete Equation 7(a) [16], and to calculate the strain corresponding to the concrete strength, Equation 7(b) [24] were considered.

$$E_c = 4700\sqrt{f_c'} \tag{7-a}$$

$$\varepsilon_c' = 1.7\ \frac{f_c'}{E_c} \tag{7-b}$$

Once the calculation of mid-height displacement is concluded for one load step, the load step increases, and the same procedure would be repeated for different load steps up to the peak load. The criterion which determine the peak load is defined when the required moment at the mid-height of the column (i.e. $M = Pe_0 + P\delta$) exceeds the capacity of the moment-curvature diagram built for that certain load (P). Once the latter happens, the procedure to finding the load step refines by decreasing the load step and repeating the procedure from the last valid found load and displacement set. Eventually, when the peak load is determined, the same procedure will be proceeds to find the nodes for the descending branch by using descending load steps. It should be noted that for the descending branch, the repetition of the iterative procedure would result in finding the nodes on the ascending branch if proper restrictions are not defined. The restrictions for descending branch are the curvature and displacement at the mid-height which must be found to be greater than the previous load step.

In addition, the axial load-bending moment interaction diagram can be built using the section analysis explained earlier by the difference that the criteria are crushing of the concrete in compression, crushing of the FRP in compression, or rupture of FRP in tension. Firstly, the ultimate concrete fiber in compression is set to be 0.003 mm/mm (or 0.0035 mm/mm) as the crushing strain of concrete for design purposes defined by ACI 318 [16] (or CSA A23.3 [17]). Then the depth of neutral axis could vary to give different sets of axial loads and bending moments by satisfying load and moment equilibrium for each different depth of neutral axis. Secondly, the crushing of FRP must be considered to see if in any case the strain in the compressive FRP layer exceeds the crushing strain or not. It should be noted that since in general the crushing strain of

FRPs are higher than 0.003 mm/mm or (0.0035 mm/mm), there would be no crushing criterion for FRPs in practice and for design purposes up to ultimate design load. The third criterion is the rupture of the FRP layers in tension which can be achieved by determining the balance point. The balance point in this case is the point in the axial load-bending moment interaction diagram at which the crushing of ultimate compressive fiber in concrete and the rupture in the ultimate tensile FRP layer happens simultaneously. Above the balance point, the crushing of concrete is the controlling criterion and below that the rupture of FRP is controlling criterion. For determining the points below the balance point, the strain at the ultimate tensile FRP layer is set to the tensile rupture strain of FRP, which is determined from material test, and the depth of neutral axis alters which gives the remaining sets of axial loads and bending moments to complete the interaction diagram.

4.2. Model Verification

The described numerical-analytical model was verified by the experimental test results presented in this paper as well as another experimental result [8] for a study performed on slender concrete columns reinforced with NSM CFRP strips. For verification of the model, two different modulus of elasticity and strength for CFRP strips in compression and tension were considered as explained in section 3. It should be noted that to obtain axial load-bending moment interaction diagram, the crushing strain of concrete in compression was considered as 0.003 mm/mm. Overall, the results of the analysis of the strengthened columns using the describe model, versus the average of experimental test data, are presented in Figure 11. The graphs for the average of experimental test data was obtained using the test results from Figure 7. It should be noted that because there were two or three graphs for averaging and they did not finish at the same value on the horizontal axis, once one of the graphs was concluded, the average shows the average of the remaining curves.

The test results show a good agreement between the model and experimental test data. It should be noted that the slope of load-displacement curve for eccentricity-to-width ratio of 0.3 is different because of possible inaccuracies in the experimental measurement for the lateral displacement [Figure 1(c)], the same issue appears in the moment-curvature [Figure 1(d)].

Table 3 shows the values of peak loads for different eccentricities as well as the corresponding displacement, bending moment, compressive and tensile strain, and the curvature of the columns. It should be noted that this time instead of averaging a graph, the peak loads and their corresponding values for displacement and etc. were considered for averaging. The results show and average of 9% error at the peak load. Moreover, as shown in both Table 3 and Figure 11, the model is in a better agreement when is used to predict the behavior of the specimens with lower load-eccentricities. However, as shown in Figure 11(d), the loading path is predicted accurately for all specimens up to the axial load-bending moment interaction diagram.

Furthermore, the loading path of the model was verified versus an experimental test result from a study performed on slender concrete columns strengthened with NSM CFRP strips by Gadjosova [8]. There were two similar specimens named “C3” and “C4” which rectangular columns (210 mm × 150 mm) tested under the same load eccentricities of 40 mm at both ends. There were two layers of steel reinforcement (4 Φ10) located at 31 mm from the edge of concrete symmetrically. There were three grooves (3 mm × 15 mm) on each side of the concrete columns containing three CFRP strips (1.4 mm × 15 mm). The modulus of elasticity and strength of steel rebar were reported as 560 MPa and 208 GPa, respectively, while these values were 2500 MPa and 168 GPa for CFRP. It should be noted that the modulus of elasticity was considered the same in tension and compression, however, the compressive strength of the CFRP material was considered to be equal to one third of its tensile strength to be compatible with the observations of

this study in the experimental part. The results of the analysis using the model described in this paper and the mentioned test data is presented in Figure 11. The results for the loading path shows a good agreement between the test data and the model. Therefore, the introduced model was used to perform a parametric study to further investigations presented in the following sections.

4.3. Parametric Studies

In this section further investigations were done for CFRP NSM strengthening system on the behavior of concrete columns by altering the reinforcement ratio and the concrete strength. It should be noted that in the parametric study section all the parameters are the same as the ones introduced in section 3 for the experimental test, however, the eccentricity-to load ratio is kept as 0.2 as the reference.

4.3.1. Effect of Reinforcement Ratio

In this section, the thickness of the CFRP strips used for strengthening was double and tripled without changing the height and their position in the experimental concrete specimens. Therefore, three reinforcement ratios of 0.21% (4×1.2 mm×10 mm), 0.43% (4×2.4 mm×10 mm), and 0.64% (4×3.6 mm×10 mm) were considered in the parametric study. The model was implemented for the cases and the results are shown in Figure 12. The results showed 4.32% and 8.61% gain in the capacity of the specimens as the reinforcement ratio increased from 0.21% to 0.43% and 0.64%, respectively. It should be noted that the interaction diagram enlarges in tension control region as the reinforcement increases as is presented in Figure 12(d). Moreover, there would be no rupture of CFRP strips in the tension control side of the interaction diagram by increasing the reinforcement ratio [Figure 12(d)], since there is a balance point for reinforcement ratio of 0.21% while for the other reinforcement ratios there is no observation of balance point. Furthermore, the compressive strain of the CFRP strips at peak load was less than 50% of the expected crushing

strain of the CFRPs (i.e. 43%, 46%, and 48% of the crushing strain of CFRP for 0.21%, 0.42%, and 0.64% reinforcement ratios, respectively) which is in an agreement with the observations from the experimental test results [Figure 12(b)].

For further studies on a higher level of compressive strain that might be experienced, the reinforcement ratio varied from 0.21% (the same as experimental study) up to 1.5% as presented in Figure 13. To observe further effects, in addition to the concrete strength of 37 MPa (the same as experimental study), a higher concrete strength of 50 MPa was examined. The results show that as the reinforcement ratio increases, the compressive strain of CFRP strips at peak load increases. However, after a certain reinforcement ratio, which is 1.7% for 37 MPa concrete strength and 2.5% for 50 MPa concrete strength, respectively, the compressive strain at peak load does not increase as the reinforcement ratio increases. It was observed that the ratio of CFRP compressive strain at the peak load to the crushing strain varies from 43% to 64% and from 50% to 69% for 37 MPa and 50 MPa concrete strength, respectively. It should be noted that if the reinforcement ratio increases, in theory, the compressive CFRP strain equal to the crushing strain will achieve. However, practically the range of reinforcement ratio that might be used for strengthening may not exceed 1% which is corresponding to strain levels that were equal to 54% and 61% of the crushing strain of CFRP strips for 37 MPa and 50 MPa concrete strength, respectively. Therefore, crushing would not happen at the peak load.

4.3.2. Effect of Concrete Strength

To find out the effect of concrete strength, three different concrete strength of 25 MPa, 35 MPa, and 45 MPa for two different reinforcement ratios of 0.21% and 0.64% were considered, as shown in Figure 14 and Figure 15. The compressive strain of the CFRP strips in compression at peak load were 36%, 42%, and 48% of the material crushing strain for 25 MPa, 35 MPa, and 45 MPa concrete

strength for reinforcement ratio of 0.21%, respectively, and 42%, 47%, and 52% for reinforcement ratio of 0.64%. The latter shows that compressive CFRP strips experience more strains as concrete strength increases, however, their peak load strain is still less than 50% of their compressive crushing strain. For all the specimens, as concrete strength increases, the strength of specimen increases, however, for 0.21% reinforcement ratio the gain is axial capacity was more than the gain for 0.64% reinforcement ratio for specimens with respect to the specimen with 25 MPa concrete strength.

It should be noted that there is a difference in the axial load- bending moment interaction diagram of the specimens with 0.21% [Figure 14(d)] and 0.64% [Figure 15(d)] reinforcement ratios. In Figure 14(d), as the concrete strength increases, the balance point (the point at which the extreme compressive fiber in concrete reaches the strain level of 0.003 mm/mm, as the defined crushing strain, and the tensile CFRP reaches its rupture strain) occurs at higher load levels which cause tension rupture of CFRP. This controls the lower part of the interaction diagram shown as a line below the balance point for specimens with 35 and 45 MPa concrete strength [Figure 14(d)]. However, by increasing the reinforcement ratio from 0.21% to 0.64%, there is no observation for the same range of concrete strength [Figure 15(d)]. Therefore, an increase in concrete strength might result in the appearance of the rupture of tensile CFRPs in the interaction diagram which can be avoided by increasing the reinforcement ratio.

To justify the observation, consider the internal forces created in the concrete and FRP strips to satisfy the force and moment equilibrium in the section. If the concrete strength increases the depth of the neutral axis tends to decrease since the required internal compressive force in concrete to satisfy force equilibrium demands less concrete area in compression. Then, the shallower depth of neutral axis causes higher tensile strains in tensile CFRP strips, which makes it

susceptible to experience rupture. Thus, an increase in concrete strength may lead to tensile rupture of CFRP strips. However, if the reinforcement ratio increases, the internal tensile force created by tensile CFRP strips increases which demands more area of concrete to be stressed in compression for satisfying force equilibrium in the section which leads to deeper depth of neutral axis. Therefore, the CFRP strips in tension side experience lower strains which might avoid the occurrence of their tensile rupture in the interaction diagram. To examine the above explanation, a range of 0.21% to 3.2% reinforcement ratios were considered for four different concrete strength of 25, 35, 45, and 55 MPa to see how the balance point can be affected for a wider range of reinforcement ratio and concrete strength, as shown in Figure 16. This observation shows that the balance load is negative for higher reinforcement ratios and higher concrete strength which equals to elimination of the rupture of CFRP strips in tension.

5. CONCLUSIONS

In this study, the behavior of the short concrete columns reinforced with longitudinal NSM CFRP laminates were investigated using experimental and analytical methods. A total of fourteen reinforced concrete specimens were prepared and tested under four different load eccentricities of 0, 10%, 20%, and 30% of the width of the specimen. Furthermore, an analytical model was developed and verified against the available experimental test data which led to a parametric study. The following conclusions can be drawn:

- The results of the material coupon tests on the CFRP laminates used in this study showed that both compressive and tensile stress-strain curves are linear for this material up to crushing in compression or rupture in tension. The compressive to tensile strength, modulus of elasticity, and ultimate strain ratios for the tested coupons were 34%, 86%,

and 40%, respectively. It should be noted that even ratio of 0.34 for compressive to tensile strength of CFRP still gives a compressive strength twice greater than conventional structural steel.

- Four modes of failure were observed in reinforced specimens consisting of concrete spalling (CS), concrete crushing (CC), compressive FRP crushing (CFC), tensile FRP rupture (TFR), however, no buckling or debonding of NSM FRP strips observed during the tests. It should be noted that no crushing or rupture of CFRP strips were observed until long after the peak load.
- The average compressive strain of CFRP strips for all concrete specimens under eccentric loading was only 41% and 84% of their crushing strain at peak load and after 15% drop from the peak load, respectively. This indicates that crushing of the CFRP strips is not a concern for the specimens considered in this study.
- For experimental test data with CFRP reinforcement ratio of 0.21%, the load capacities of the strengthened specimens were improved by 7.7% and 10.9% of the capacity of the plain concrete tested under pure compression and under eccentricity-to-width ratio of 10%, respectively.
- The results of parametric study showed that as the reinforcement ratio increases, the compressive strain of CFRP laminates in compression increases. However, in a practical range of reinforcement ratio (considering less than 1% reinforcement ratio), the CFRP strain level at peak load does not reach the crushing value. It was observed that the stain levels in compressive CFRP strips were equal to 54% and 61% of their crushing strain of CFRP strips for 37 MPa and 50 MPa concrete strength, respectively, for the eccentricity-to-width ratio of 20%.

- It was observed by the parametric study that as the concrete strength increases from 25 MPa to 45 MPa, the CFRP compressive strain at the peak load increases. However, the strain of compressive CFRP strips did not pass 50% of their crushing strain per coupon tests.
- Overall, this study showed that for short concrete columns strengthen with NSM CFRP laminates, crushing, buckling, or debonding failures of CFRP laminates in compression did not affect the load capacity of the columns and crushing of CFRP strips happened long after peak loads. The results showed that the strengthening of concrete columns using longitudinal NSM FRPs is a viable approach. Further studies are needed to implement the system enhancing the performance of slender columns through increasing their lateral stiffness.

6. ACKNOWLEDGEMENT

The authors would like to thank Blair Nickerson, Brian Kennedy, Jesse Keane, and Brian Liekens of Dalhousie University for their assistance in the lab. The authors would also like to acknowledge and thank NSERC and Dalhousie University for their financial support. Randy Nason of Pinnacle Agencies Ltd (Dartmouth, NS, Canada) is thanked for providing the BASF adhesive. Finally, authors specially thank Dr. Farid Taheri for his precious technical guidance in material testing and Dr. John Newhook for providing Sika CFRP laminates and his support for the tests.

7. REFERENCES

[1] M. Badawi and S. Khaled, "Flexural strengthening of RC beams with prestressed NSM CFRP rods – Experimental and analytical investigation," *Construction and Building Materials,* vol. 23, no. 10, pp. 3292-3300, 2009.

[2] F. Ceroni, "Experimental performances of RC beams strengthened with FRP materials," *Construction and Building Materials,* vol. 24, no. 9, pp. 1547-1559, 2010.

[3] H. Nordin and B. Täljsten, "Concrete Beams Strengthened with Prestressed Near Surface Mounted CFRP," *Journal of Composites for Construction,* vol. 10, no. 1, pp. 60-68, 2006.

[4] J. G. Teng, L. D. Lorenzis, B. Wang, R. Li, T. N. Wong and L. Lam, "Debonding Failures of RC Beams Strengthened with Near Surface Mounted CFRP Strips," *JOURNAL OF COMPOSITES FOR CONSTRUCTION,* vol. 92, no. 105, pp. 92-105, 2006.

[5] K. Khorramian and P. Sadeghian, "Strengthening Concrete Columns Using Near Surface Mounted (NSM) Carbon Fiber Reinforced Polymer (CFRP) Laminates," in *Sixth Asia-Pasofoc conference on FRP in Structures,* Singapore, Singapore, 2017.

[6] G. Foret and O. Limam, "Experimental and numerical analysis of RC two-way slabs strengthened with NSM CFRP rods," *Construction and Building Materials,* vol. 22, no. 10, pp. 2025-2030, 2008.

[7] . D. A. Bournas and T. C. Triantafillo, "Flexural Strengthening of Reinforced Concrete Columns with Near-Surface-Mounted FRP or Stainless Steel," *ACI Structural Journal,* vol. 106, no. 4, pp. 495-505, 2009.

[8] K. Gadjosova and J. Bilcik, "Full-scale testing of CFRP-strengthened slender reinforced concrete columns," *Journal of composites for construction,* vol. 17, pp. 239-248, 2013.

[9] J. A. Barros, R. K. Varma, J. M. Sena-Cruz and A. F. Azevedo, "Near surface mounted CFRP strips for the flexural strengthening of RC columns: Experimental and numerical research," *Engineering Structures*, vol. 30, no. 12, pp. 3412-3425, 2008.

[10] Fib Bulletin 14, "Externally bonded FRP reinforcement for RC structures," the International Federation for Structural Concrete, Stuttgart, 2001.

[11] ACI 440.2R, "Guide for the Design and Construction of Externally Bonded FRP Systems for Strengthening Concrete Structures," American Concrete Institute, Farmington Hills, MI, 2008.

[12] CAN/CSA S806-12, "Design and construction of building structures with fibre-reinforced polymers," Canadian Standards Association, 2012.

[13] P. Sadeghian and . A. Fam, "Strengthening slender reinforced concrete columns using high-modulus bonded longitudinal reinforcement for buckling control," *Journal of structural Engineering*, vol. 141, p. 04014127, 2015.

[14] ASTM D3039/D3039M-14, "Standard Test Method for Tensile Properties of Polymer Matrix Composite Materials," American Society for Testing and Materials, West Conshohcken, PA, 2014.

[15] ASTM D6641/D6641M-16, "Standard Test Method for Compressive Properties of Polymer Matrix Composite Materials Using a Combined Loading Compression (CLC) Test Fixture," American Society for Testing and Materials, West Conshohocken, PA, 2016.

[16] ACI 318-14, "Building Code Requirements for Structural Concrete," American Concrete Institute, Farmington Hills, MI, 2014.

[17] CAN/CSA A23.3-14, "Design if concrete structures," Canadian standard association, 2014.

[18] E. Hognestad, "A Study of Combined Bending and Axial Load in Reinforced Concrete Members, Bulletin Series No. 399," University of Illinois, Urbana, 1951.

[19] B. Broms and M. I. Viest, "Long Reinforced Concrete Columns: A symposium," *Transactions, ASCE,* vol. 126, no. 2, pp. 308-400, 1961.

[20] A. N. Lloyd and V. B. Rangan, "Studies on High-Strength Concrete Columns under Eccentric Compression," *ACI Structural Journal,* vol. 93, no. 6, pp. 631-638, 1996.

[21] C. Claeson and . K. Gylltoft, "Slender High-Strength Concrete Columns Subjected to Eccentric Loading," *Journal of Structural Engineering,* vol. 124, no. 3, pp. 233-240, 1998.

[22] A. Mirmiran, W. Yuan and X. Chen, "Design of Slenderness in Concrete Columns Internally Reinforced with Fiber-Reinforced Polymer Bars," *ACI Structural Journal,* vol. 98, no. 1, pp. 116-125, 2001.

[23] S. Popovics, "A numerical approach to the complete stress-strain curve of concrete," *Cement and concrete research,* vol. 3, no. 5, pp. 583-599, 1973.

[24] C. E. Todeschini, A. C. Bianchini and C. E. Kesler,, "Behavior of Concrete Columns Reinforced with High Strength Steels," *ACI Journal,* vol. 61, no. 6, pp. 701-716, 1964.

Table 1. Test specimen properties.

No.	Specimen ID	Eccentricity ratio, e/h (%)	Eccentricity, e (mm)	Reinforcement
1	N-e0-1	0	0	CFRP
2	N-e0-2	0	0	CFRP
3	N-e10-1	10	15	CFRP
4	N-e10-2	10	15	CFRP
5	N-e10-3	10	15	CFRP
6	N-e20-1	20	30	CFRP
7	N-e20-2	20	30	CFRP
8	N-e30-1	30	45	CFRP
9	N-e30-2	30	45	CFRP
10	P-e0-1	0	0	None
11	P-e0-2	0	0	None
12	P-e10-1	10	15	None
13	P-e10-2	10	15	None
14	P-e10-3	10	15	None

Table 2. Summary of test results

No.	Specimen ID	Peak Load, P_u (kN)	SG1 at peak load (mm/mm)	SG1 at peak load to rupture strain ratio	SG2 at peak load (mm/mm)	SG2 at peak load to crushing strain ratio	SG1 at 0.85 P_u (mm/mm)	SG1 at 0.85 P_u to rupture strain ratio	SG2 at 0.85 P_u (mm/mm)	SG2 at 0.85 P_u to crushing strain ratio
1	N-e0	774.5	-0.00197	-0.12	-0.00156	0.24	-	-	-	-
2	N-e10	661.2	-0.00004	0.00	-0.00280	0.42	0.00059	0.04	-0.00568	0.86
3	N-e20	545.0	0.00058	0.03	-0.00329	0.50	0.00111	0.07	-0.00508	0.77
4	N-e30	398.9	0.00239	0.14	-0.00327	0.50	0.00480	0.29	-0.00591	0.90
5	P-e0	719.2	-	-	-	-	-	-	-	-
6	P-e10	596.3	-	-	-	-	-	-	-	-

Note: CFRP strains were recorded by SG1 (tension side) and SG2 (compression side), as shown in Figure 3; the sign convention is positive for tensile strains and negative compressive strains; rupture strain = 0.01668 mm/mm; crushing strain =0.0066 mm/mm.

Table 3. Comparison of model and experimental results

Characteristic	e/h (%)	Test	Model	Test to model ratio	Test to model ratio (AVG±SD)
Peak Load (kN)	10	628.4	636.7	0.98	1.15±0.02
	20	542.7	481.7	1.13	
	30	397.4	341.7	1.16	
Lateral mid-height displacement at peak load (mm)	10	0.76	0.59	1.29	1.49±0.32
	20	1.04	0.79	1.32	
	30	2.20	1.19	1.85	
Compressive strip strain at peak load (mm/mm)	10	-0.00280	-0.00284	0.99	1.11±0.10
	20	-0.00329	-0.00285	1.14	
	30	-0.00327	-0.00301	1.19	
Moment at peak load (kN-m)	10	9.9	9.9	1.00	1.11±0.10
	20	16.8	14.8	1.14	
	30	18.8	15.8	1.19	
Curvature at peak load (1/km)	10	16.3	19.7	0.83	0.97±0.12
	20	28.4	26.6	1.07	
	30	40.8	41.0	1.00	

Note: e/h is the load eccentricity to width ratio; AVG=average; and SD=standard deviation.

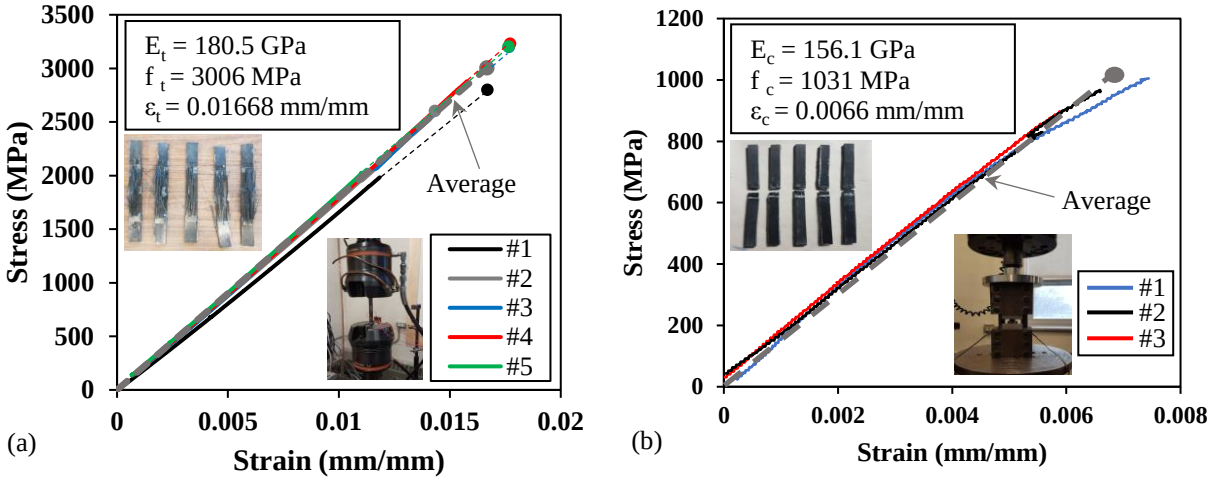

Figure 1. Experimental stress-strain curves of CFRP laminates in (a) tension and (b) compression.

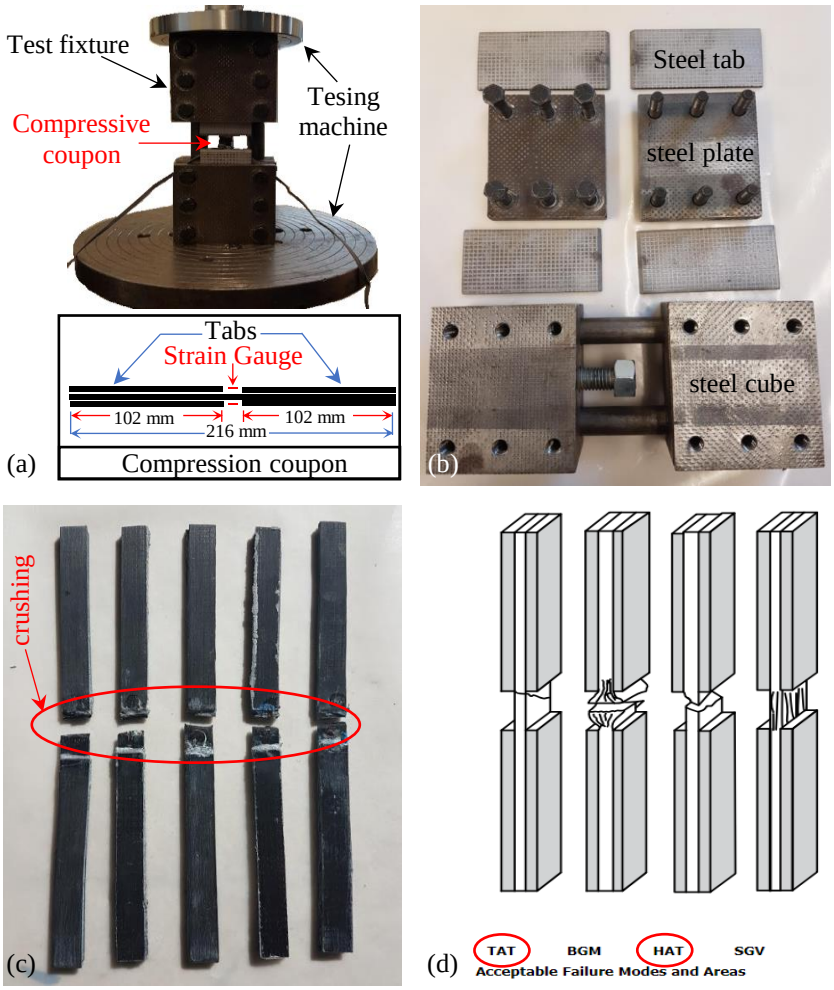

Figure 2. Compression coupon test: (a) compressive coupon and test set-up; (b) Test fixture components; (c) broken specimen; and (d) accepted failure modes by ASTM D6641 [15].

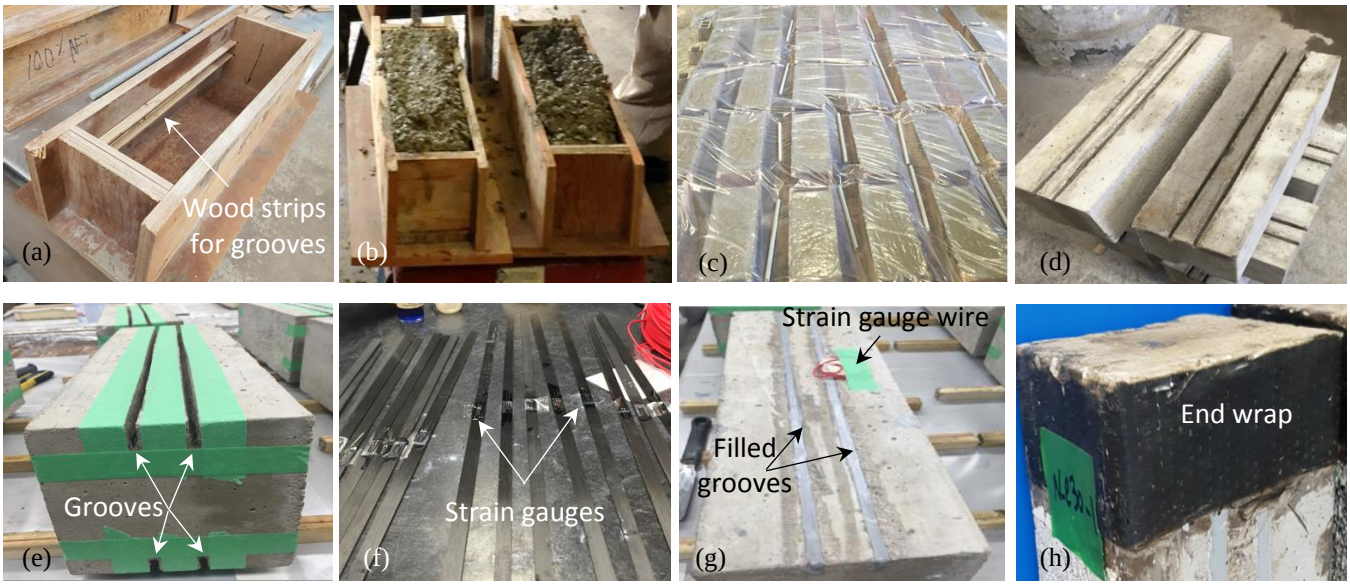

Figure 3. Specimen fabrication: (a) mold; (b) fresh concrete; (c) curing; (d) concrete specimens; (e) prepared grooves; (f) CFRP strips; (g) filled grooves; and (h) end wrap.

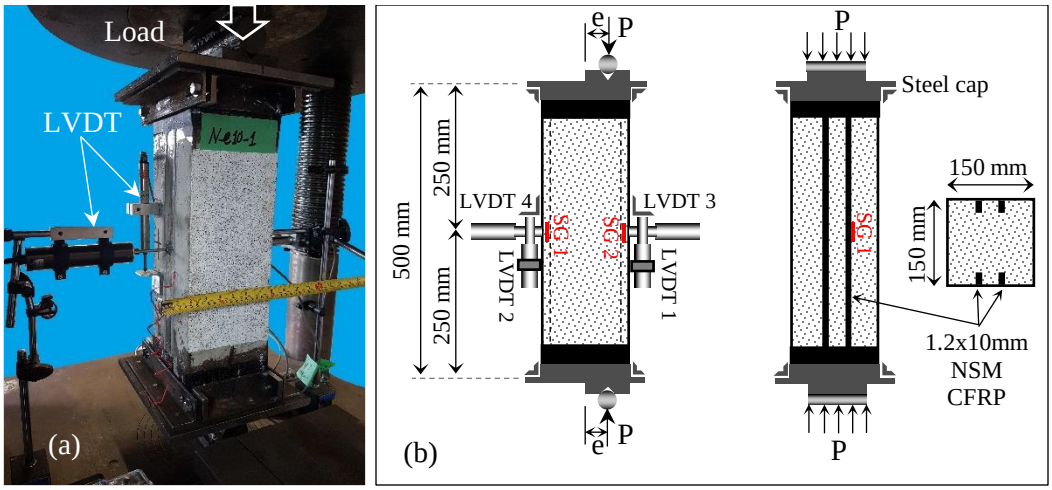

Figure 4. Test set up and instrumentation: (a) testing machine and instrumentation, and (b) schematic testing specimen and reinforcement layout.

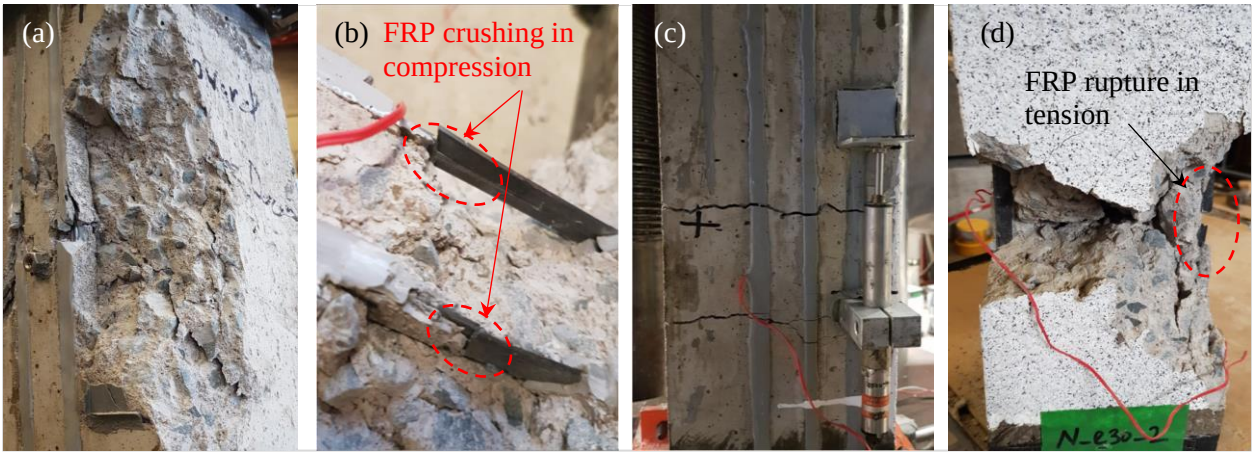

Figure 5. Modes of failure: (a) concrete spalling (CS); (b) compressive FRP crushing (CFC); (c) tensile cracks; and (d) tensile FRP rupture (TFR).

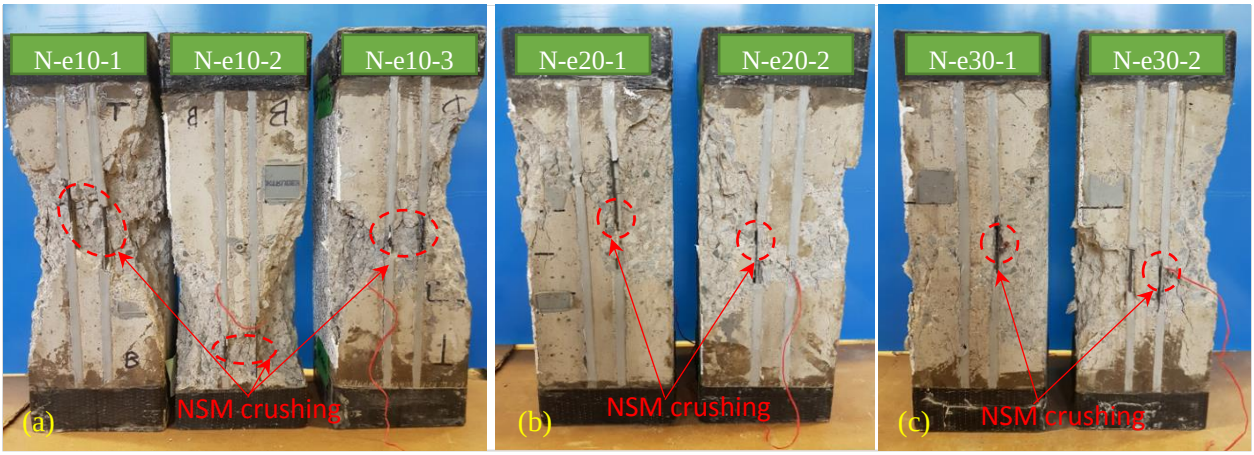

Figure 6. Compressive side of tested specimens: (a) e10 group; (b) e20 group; and (c) e30 group.

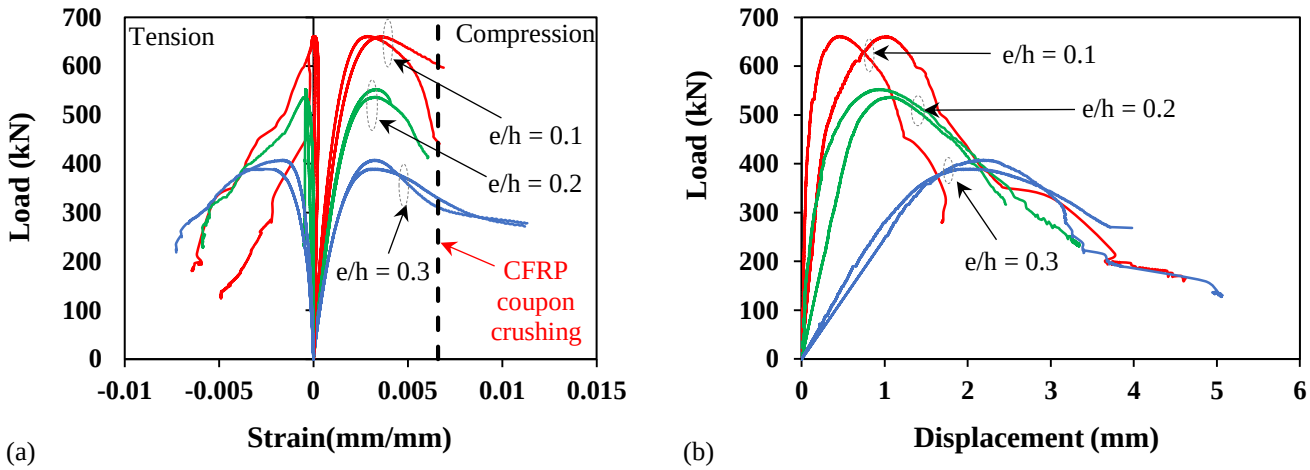

Figure 7. Test results: (a) axial load vs. strain of compressive and tensile CFRP strips; and (b) axial load vs. lateral displacement of specimens at mid-height.

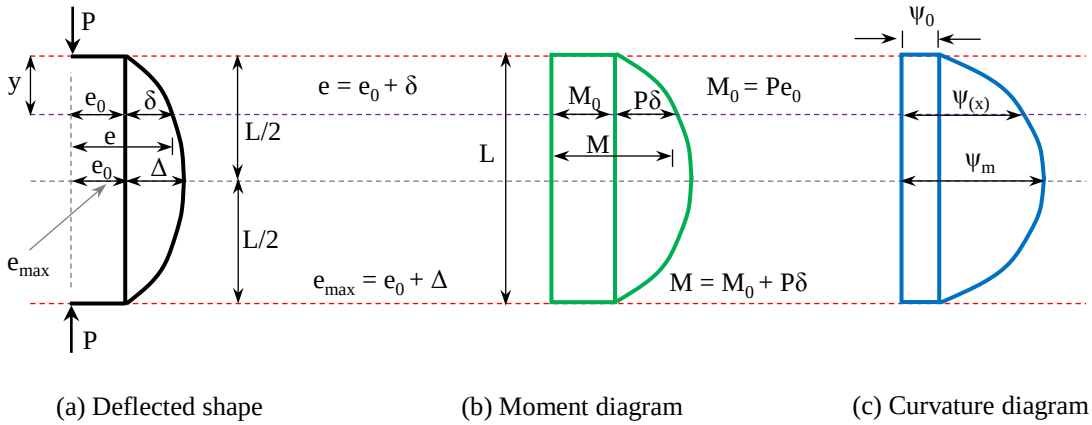

(a) Deflected shape (b) Moment diagram (c) Curvature diagram

Figure 8. Schematic illustration of iteration process: (a) deflected shape of column; (b) moment diagram; and (c) curvature diagram.

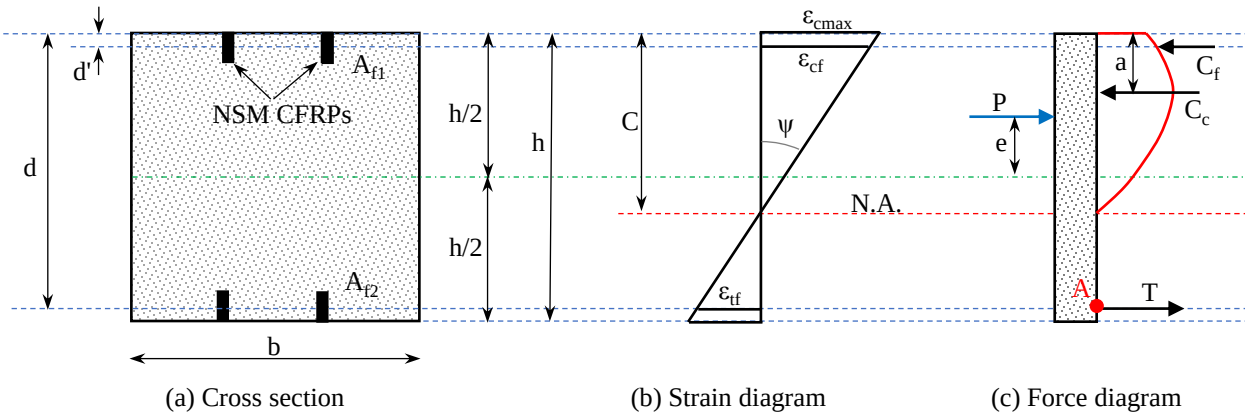

(a) Cross section (b) Strain diagram (c) Force diagram

Figure 9. Mechanism of cross-sectional analytical model: (a) section definitions; (b) strain diagram; and (c) force diagram.

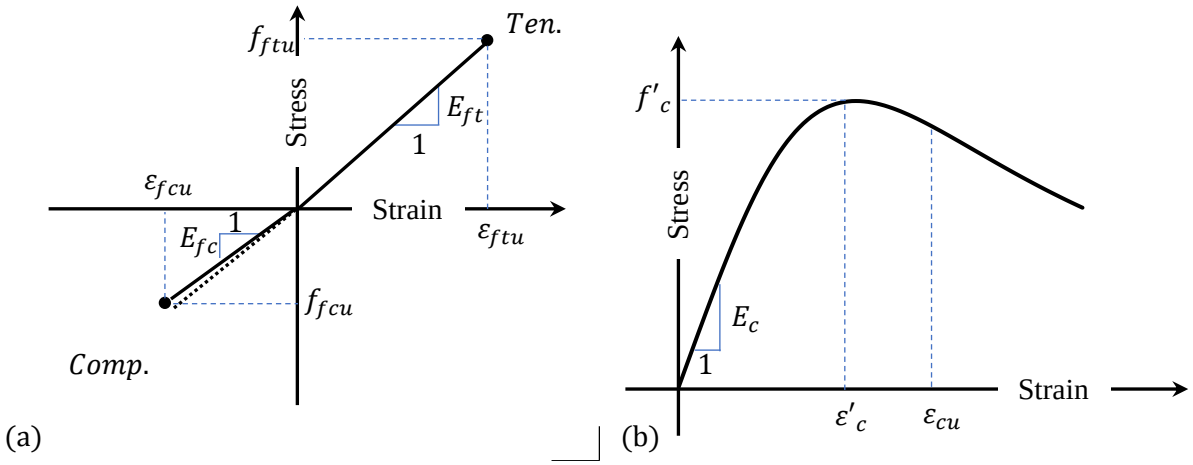

Figure 10. Material properties for model: (a) stress-strain curve of CFRP laminate in tension and compression; (b) stress-strain curve of concrete in compression.

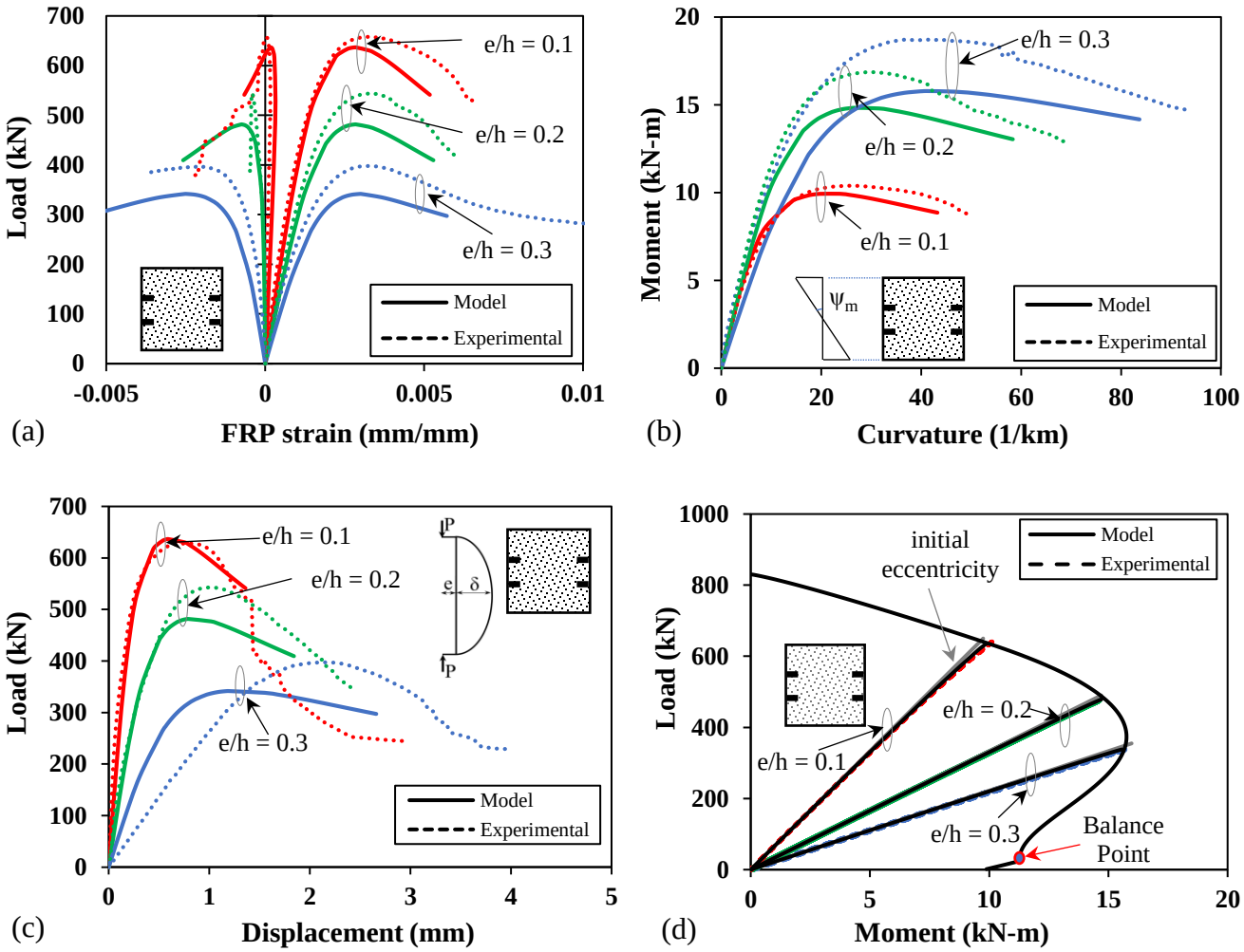

Figure 11. Model verification: (a) axial load vs. strain of compressive and tensile CFRP strips; (b) moment vs. curvature diagram at the mid-height; (c) axial load vs. lateral displacement of specimens at mid-height; and (d) axial load vs. bending moment interaction diagram and loading path curves.

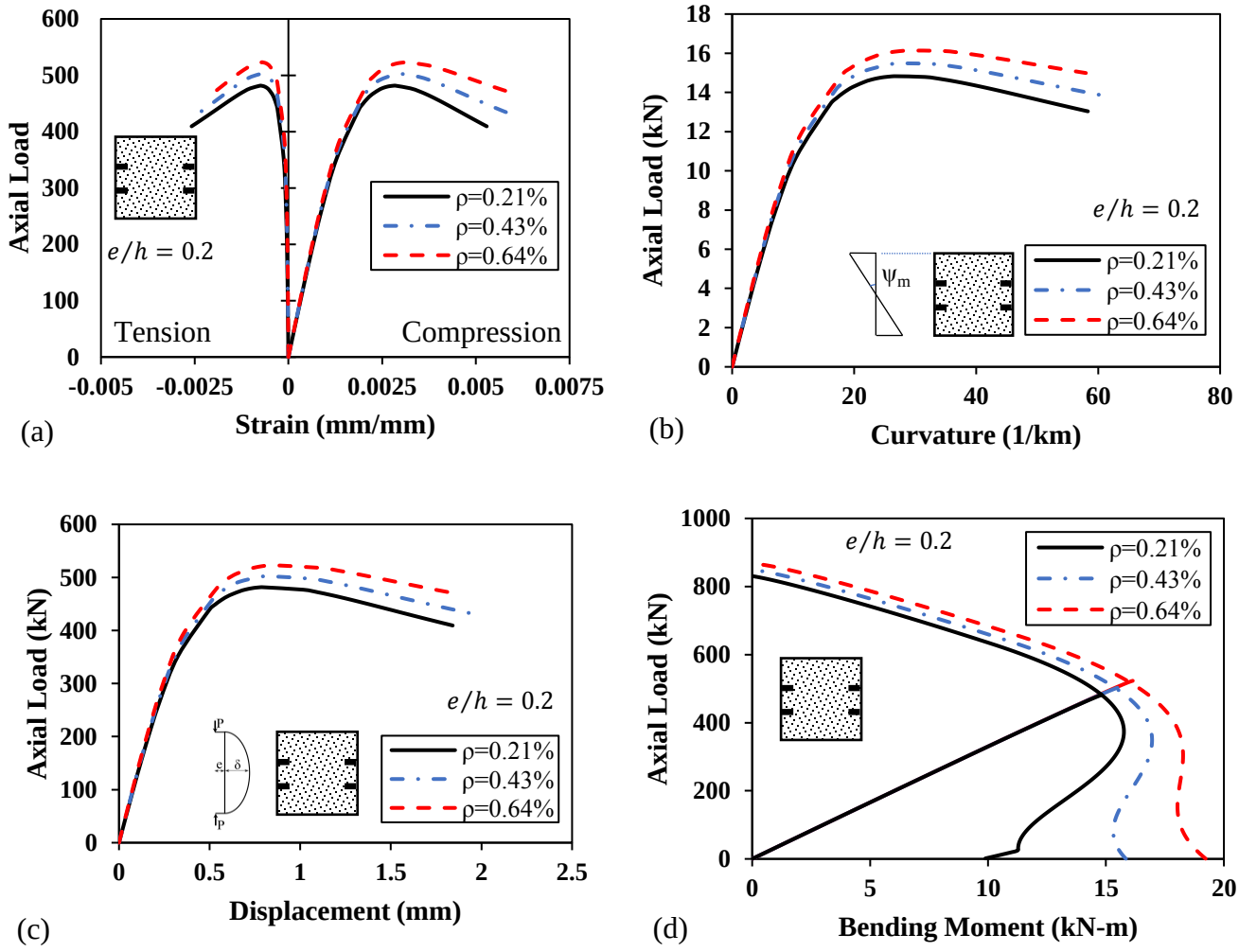

Figure 12. Effect of the reinforcement ratio: (a) axial load vs. strain of compressive and tensile CFRP strips; (b) moment vs. curvature diagram at the mid-height; (c) axial load vs. lateral displacement of specimens at mid-height; and (d) axial load vs. bending moment interaction diagram and loading path curves.

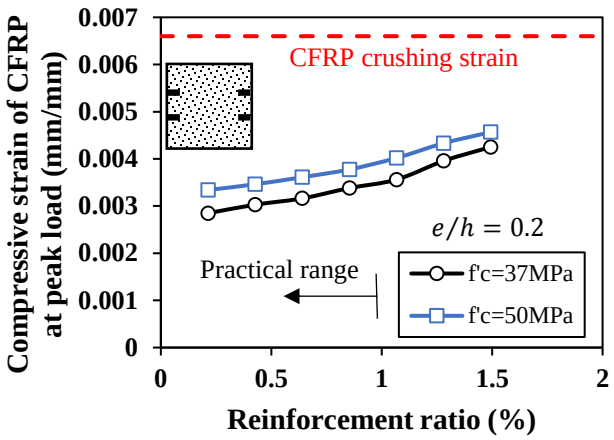

Figure 13. Reinforcement ratio vs. compressive strain of CFRP strip at peak load

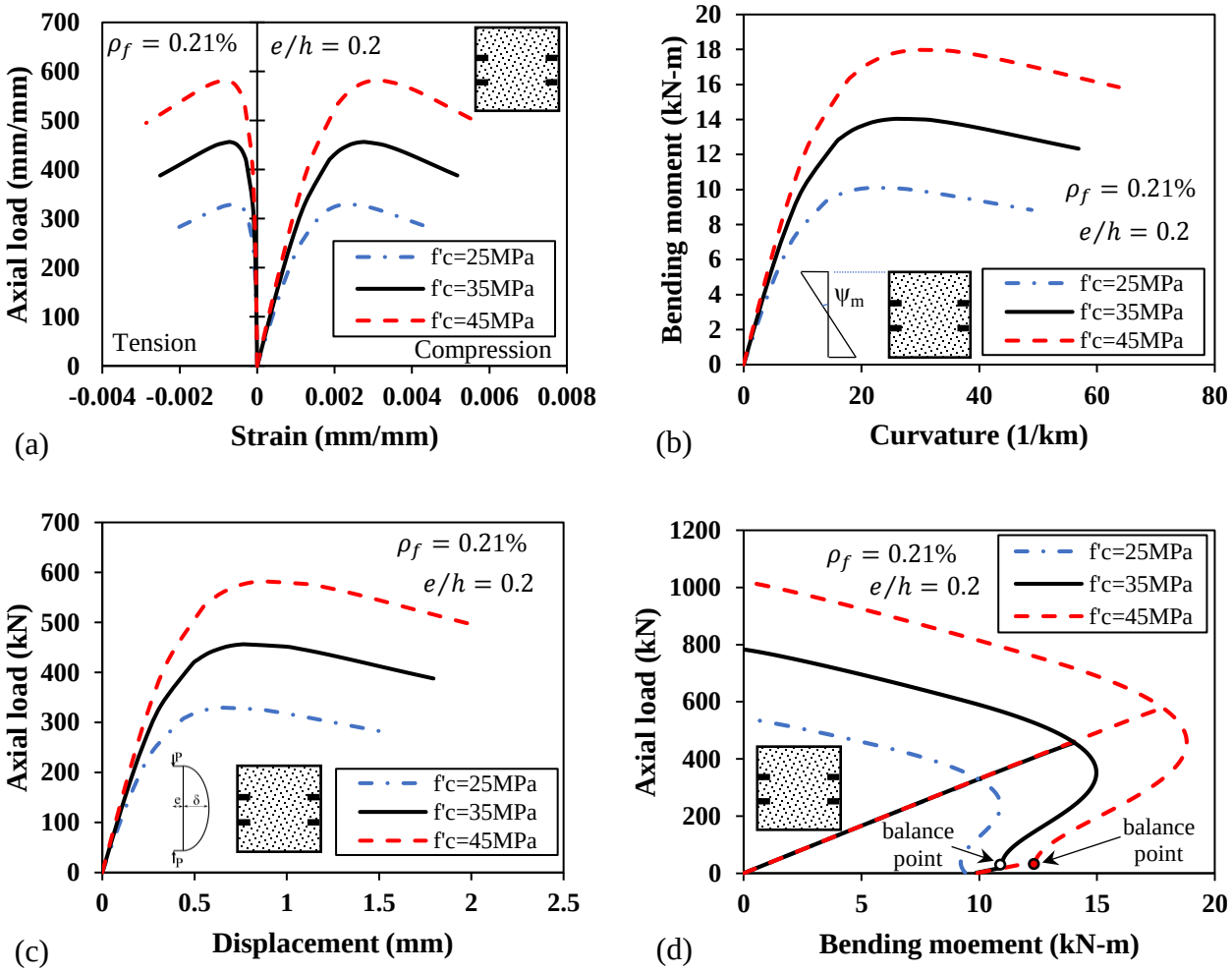

Figure 14. Effect of the concrete strength (reinforcement ratio of 0.21%): (a) axial load vs. strain of compressive and tensile CFRP strips; (b) moment vs. curvature diagram at the mid-height; (c) axial load vs. lateral displacement of specimens at mid-height; and (d) axial load vs. bending moment interaction diagram and loading path curves.

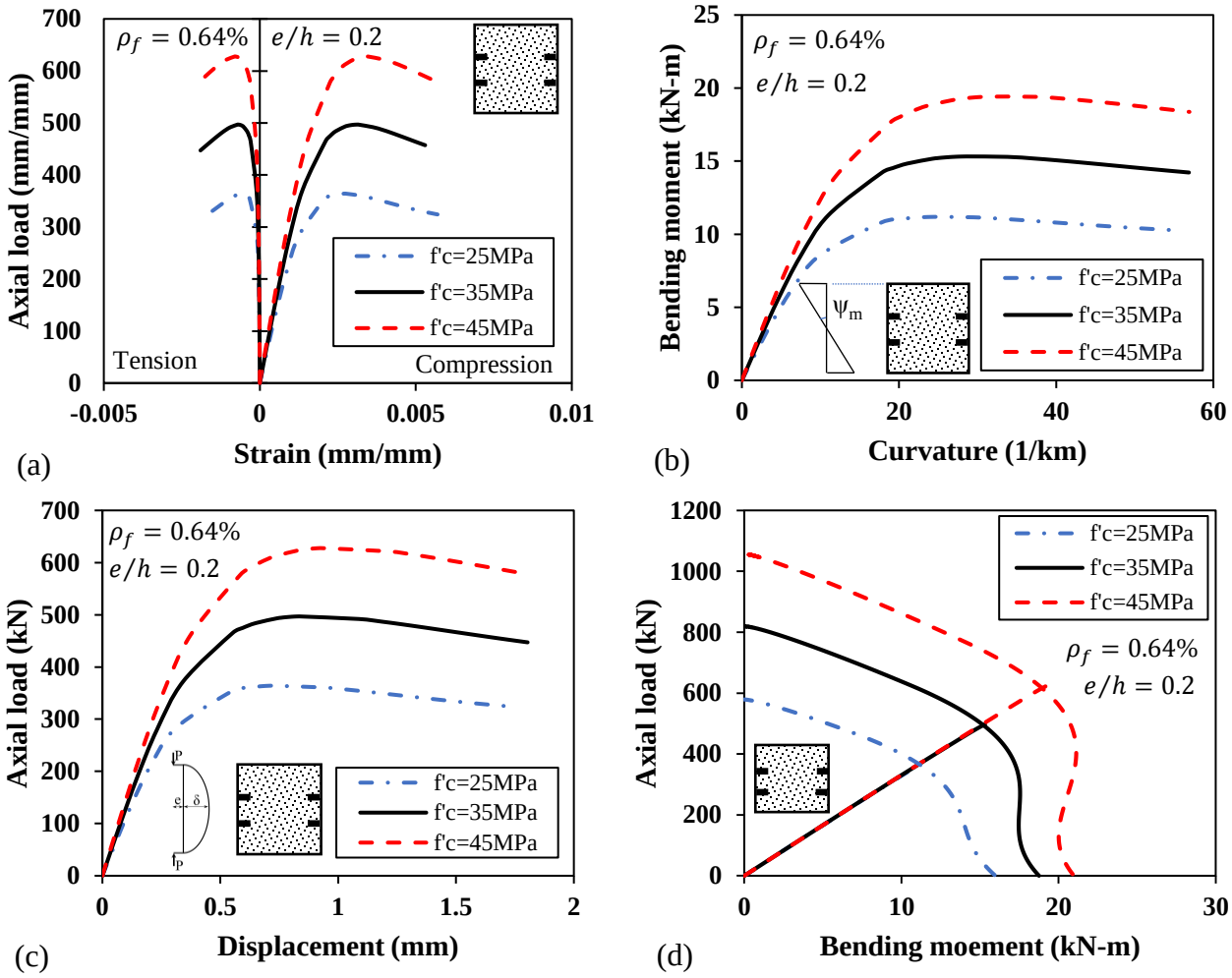

Figure 15. Effect of the concrete strength (reinforcement ratio of 0.64%): (a) axial load vs. strain of compressive and tensile CFRP strips; (b) moment vs. curvature diagram at the mid-height; (c) axial load vs. lateral displacement of specimens at mid-height; and (d) axial load vs. bending moment interaction diagram and loading path curves.

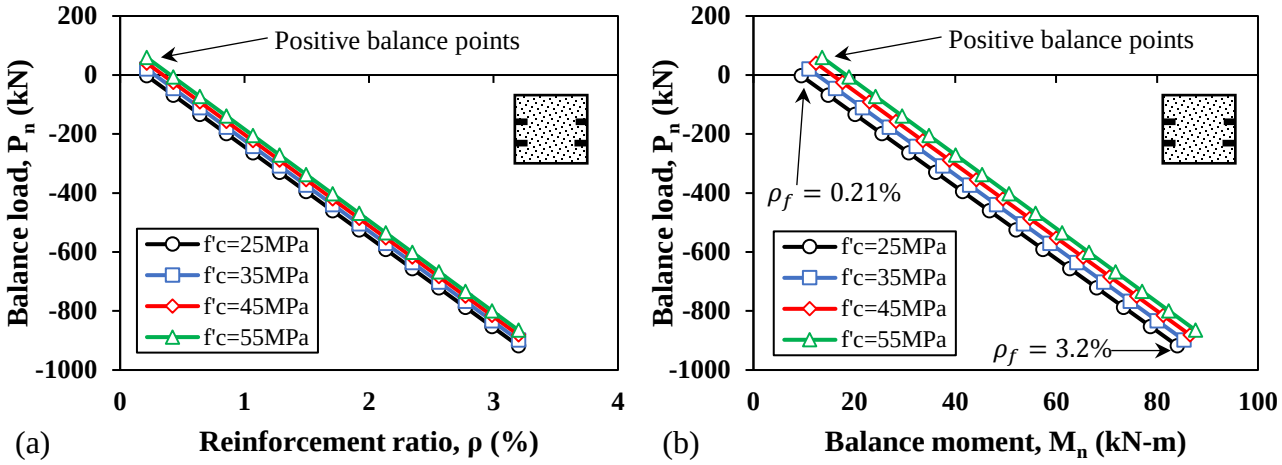

Figure 16. Balance points for interaction diagram: (a) balance load vs. reinforcement ratio and (b) balance load vs. balance moment